Available online at www.sciencedirect.com

ScienceDirect

Geochimica et Cosmochimica Acta 71 (2007) 1898–1912

Geochimica et Cosmochimica Acta

www.elsevier.com/locate/gca

Adsorption of Fe(II) and U(VI) to carboxyl-functionalized microspheres: The influence of speciation on uranyl reduction studied by titration and XAFS

Maxim I. Boyanov [a,b,*], Edward J. O'Loughlin [a], Eric E. Roden [c], Jeremy B. Fein [b], Kenneth M. Kemner [a]

[a] *Biosciences Division, Argonne National Laboratory, Argonne, IL 60439, USA*
[b] *Department of Civil Engineering and Geological Sciences, University of Notre Dame, Notre Dame, IN 46556, USA*
[c] *Department of Geology and Geophysics, University of Wisconsin-Madison, Madison, WI 53706, USA*

Received 10 July 2006; accepted in revised form 29 January 2007; available online 6 February 2007

Abstract

The chemical reduction of U(VI) by Fe(II) is a potentially important pathway for immobilization of uranium in subsurface environments. Although the presence of surfaces has been shown to catalyze the reaction between Fe(II) and U(VI) aqueous species, the mechanism(s) responsible for the enhanced reactivity remain ambiguous. To gain further insight into the U–Fe redox process at a complexing, non-conducting surface that is relevant to common organic phases in the environment, we studied suspensions containing combinations of 0.1 mM U(VI), 1.0 mM Fe(II), and 4.2 g/L carboxyl-functionalized polystyrene microspheres. Acid-base titrations were used to monitor protolytic reactions, and Fe K-edge and U L-edge X-ray absorption fine structure spectroscopy was used to determine the valence and atomic environment of the adsorbed Fe and U species. In the Fe + surface carboxyl system, a transition from monomeric to oligomeric Fe(II) surface species was observed between pH 7.5 and pH 8.4. In the U + surface carboxyl system, the U(VI) cation was adsorbed as a mononuclear uranyl–carboxyl complex at both pH 7.5 and 8.4. In the ternary U + Fe + surface carboxyl system, U(VI) was not reduced by the solvated or adsorbed Fe(II) at pH 7.5 over a 4-month period, whereas complete and rapid reduction to U(IV) nanoparticles occurred at pH 8.4. The U(IV) product reoxidized rapidly upon exposure to air, but it was stable over a 4-month period under anoxic conditions. Fe atoms were found in the local environment of the reduced U(IV) atoms at a distance of 3.56 Å. The U(IV)–Fe coordination is consistent with an inner-sphere electron transfer mechanism between the redox centers and involvement of Fe(II) atoms in both steps of the reduction from U(VI) to U(IV). The inability of Fe(II) to reduce U(VI) in solution and at pH 7.5 in the U + Fe + carboxyl system is explained by the formation of a transient, "dead-end" U(V)–Fe(III) complex that blocks the U(V) disproportionation pathway after the first electron transfer. The increased reactivity at pH 8.4 relative to pH 7.5 is explained by the reaction of U(VI) with an Fe(II) oligomer, whereby the bonds between Fe atoms facilitate the transfer of a second electron to the hypothetical U(V)–Fe(III) intermediate. We discuss how this mechanism may explain the commonly observed higher efficiency of uranyl reduction by adsorbed or structural Fe(II) relative to aqueous Fe(II).

1. INTRODUCTION

Uranium has become an environmental concern as a contaminant from power generation and defense-related activities (Riley et al., 1992; Batson et al., 1996), as well as from weathering of uranium minerals near mine tailings (Landa and Gray, 1995). To predict contaminant fate and develop remediation strategies, the factors controlling uranium speciation and reactivity must be identified and their effects evaluated for diverse environmental conditions. Aqueous ion transport in water-rock systems is usually

---

[*] Corresponding author.
E-mail address: mboyanov@nd.edu (M.I. Boyanov).

0016-7037/$ - see front matter © 2007 Elsevier Ltd. All rights reserved.
doi:10.1016/j.gca.2007.01.025

controlled by adsorption and/or precipitation reactions, which can be manipulated to contain a propagating contaminant plume. For aqueous uranium, in particular, a promising immobilization strategy is reduction and mineral formation (e.g., Langmuir, 1978). Oxidized uranium, U^{VI}, is relatively soluble and mobile, but when uranium is reduced to U^{IV}, it forms sparingly soluble minerals, and mass transport is, in general, retarded. Dissimilatory metal-reducing bacteria (DMRB) can affect the redox conditions present in the subsurface, either by enzymatically reducing U^{VI} to U^{IV} (Gorby and Lovley, 1992; Lovley and Phillips, 1992a,b; Fredrickson et al., 2000), or by producing significant amounts of Fe^{II} during dissimilatory Fe^{III} reduction (DIR) (Bell et al., 1987; Lovley et al., 1987; Kostka and Nealson, 1995; Fredrickson et al., 1998). The Fe^{II} phases resulting from DIR provide reducing capacity in natural systems (Stumm and Sulzberger, 1992), and some of the phases, such as adsorbed Fe^{II} and mixed-valence Fe^{II}/Fe^{III} minerals, are known reductants of U^{VI} (see below). The relative importance of the microbial (enzymatic) reduction vs. the abiotic (chemical) reduction of U^{VI} in natural environments is still in question, partly due to insufficient information on the mechanisms of both processes. It is therefore important to understand the controls on U^{VI} reduction by Fe^{II}.

Reduction of U^{VI} by Fe^{II} is thermodynamically favorable under a range of environmental conditions and has been the subject of recent investigations. The homogeneous reaction between hydrated U^{VI} and Fe^{II} species is kinetically inhibited and fails to occur over at least 3 days at neutral pH under anoxic conditions; however, the addition of particulate minerals under identical experimental conditions causes complete uranium removal within hours, presumably through heterogeneous reduction by adsorbed $Fe^{II}OH^+$ species (Liger et al., 1999; Fredrickson et al., 2000; Jeon et al., 2005). Structural Fe^{II} (i.e., Fe^{II} in crystalline compounds) is also capable of reducing U^{VI}. Mixed-valence $Fe^{II,III}$ oxides and hydroxides (magnetite and green rusts), Fe^{II} sulfide (pyrite), and Fe^{II}-bearing phylosilicates (micas) have been shown to reduce aqueous U^{VI} (Wersin et al., 1994; O'Loughlin et al., 2003; Ilton et al., 2004; Scott et al., 2005). The catalytic effect of surfaces is most often attributed to decreased redox potential due to complexation of the reduced species to an electron donor ligand (i.e., a ligand effect). This interpretation is based on a body of work studying the reduction of Cr^{VI} and organic contaminants by adsorbed/complexed Fe^{II} (e.g., Stumm, 1992; Schwarzenbach et al., 1997; Buerge and Hug, 1999; Strathmann and Stone, 2002; Sposito, 2004). However, recent findings indicate that electrons from adsorbed Fe^{II} can migrate inside the adsorbing ferric oxide lattice (Williams and Scherer, 2004) and that non-local redox interactions can be mediated by semiconductor surfaces, such as those of galena and pyrite (Becker et al., 2001). These results suggest that what is thought to be adsorbed Fe^{II} may actually be structural Fe^{II}, and that electron transfer may be occurring between spatially separated redox centers through a lattice conduction/hopping mechanism. Because the reduction of U^{VI} to U^{IV} requires two electrons, whereas the oxidation of Fe^{II} to Fe^{III} provides only one, the higher U^{VI} reduction rate in the presence of a surface may also be due to the enhanced ability of two separate Fe^{II} atoms to transfer electrons to an adsorbed U^{VI} atom at the same binding site. In summary, although it is well established that Fe^{II} atoms are more efficient reducers of U^{VI} in the presence of minerals than as aqueous species, the mechanism of enhanced reactivity and the reactive species in the presence of a surface remain ambiguous. Ligand effects, atomic proximity of reducing centers, and electron lattice conduction all remain possible reduction-enhancing mechanisms at a surface.

In this work, we investigated the U^{VI}–Fe^{II} redox reactivity as a function of Fe^{II} speciation in the presence of a carboxyl-functionalized surface. Although the carboxyl functionality was chosen for its relevance to cation sorption/complexation in biotic environments (Beveridge and Murray, 1980; Fein et al., 1997; Boyanov et al., 2003), our primary focus was to determine the controls and mechanisms of U^{VI} reduction by Fe^{II}. The use of a non-conducting polystyrene matrix avoided the issue of electron tunneling in the substrate that may be present in crystal oxides, and ensured the direct electron transfer between Fe and U atoms. The complexing surface provided control over the partitioning of Fe^{II} between solvated, adsorbed, and oligomerized species. Our specific goals were to (i) identify conditions under which U^{VI} reduction occurs, (ii) identify the U^{VI} and Fe^{II} species present under non-reactive conditions, (iii) identify the U^{VI} and Fe^{II} species present in Fe-only and U-only systems under reactive conditions, and (iv) analyze the reaction products and infer details about the electron transfer mechanism. We used titration experiments to provide information on H^+ release from the surface and on OH^- consumption in precipitation reactions. X-ray absorption fine structure (XAFS) spectroscopy was used to determine the average valence and molecular environment of U and Fe atoms in the hydrated solid phase. The combination of these approaches allowed us to relate speciation to reactivity in the studied system and to deduce a mechanism for the electron transfer.

2. MATERIALS AND METHODS

2.1. Latex particles, suspensions, and reagents

Carboxyl-modified polystyrene microspheres were obtained from Bangs Laboratories, Inc. The colloids are produced by co-polymerization of polystyrene and acrylic acid, resulting in uniform spherical particles (diameter deviation of several percent) with carboxyl functional groups on the surface. The size and the carboxyl functionality were chosen to emulate the cation-binding characteristics of bacterial cells. Transmission electron microscopy (TEM) confirmed the shape and narrow size distribution of the particles (Fig. EA-1 in the electronic annex). Some properties provided by the manufacturer are summarized in Table 1. The latex particles were washed 3 times in 0.5 M HCl and 2 times in distilled deionized water, then suspended in 0.03 M $NaClO_4$ or NaCl electrolyte to buffer the ionic strength. Control experiments showed that the redox properties of the system were not affected by the type of

Table 1
Properties of the carboxyl-modified colloid (catalog number PC03N), as provided by Bangs Laboratories, Inc.

Property	Value	Units
Diameter	0.92	μm
Surface area	6.153	m^2/g
Surface titration data	94.6	μeq/g
Surface density of COOH	10.8	$Å^2$/site
Density of polymer core	1.06	g/cm^3

electrolyte used. The amounts of adsorbent in the suspensions were monitored by following optical density at 600 nm, using the manufacturer's suspensions as standards. Samples for the experiments were produced from a stock suspension and then separated into crimp-sealed glass bottles. Dissolved O_2 and CO_2 were removed by bubbling N_2 through the solutions and suspensions for 40 min. The purge gas was purified by removing O_2 with an O_2 trap (model 1000, from Chromatography Research Supplies, Inc.), followed by consecutive passage through a 5% HCl solution, a 5% NaOH solution, and the 0.03 M electrolyte solution, to remove potential acid- or base-soluble impurities and introduce humidity. The mass of the purged sample bottles, measured before and after purging, showed no change. After sparging, the bottles were immediately placed in an anoxic chamber. All further operations were carried out under an O_2-free atmosphere.

The 0.3 M stock Fe^{2+} solution was prepared by using $FeCl_2{\cdot}4H_2O$ obtained from Aldrich Chemical, Inc. To maintain the dissolved Fe as Fe^{II}, metallic Fe powder and HCl was added, the bottle was crimp-sealed, and the solution was boiled for 1 h during purging with purified N_2 gas. An aliquot for the experiment was filtered through a 0.22-μm filter in the anoxic chamber and analyzed for Fe^{II} content (final pH 3.0, [Fe] = 0.3 M). Dissolved oxygen, total Fe, and possible Fe^{3+} content in the solution were monitored by using methods described below. These procedures were used before each set of experiments to refresh the stock solution, which was kept in the dark and used under anoxic conditions within 2 days. Aqueous U^{VI} was added from an acidified uranyl chloride stock solution (pH 2.0, [U] = 0.01 M), prepared by dissolving UO_3 (obtained from STREM Chemicals, Newburyport, MA) in HCl and diluting to known volume.

2.2. Oxygen and carbon dioxide exclusion

Great care was taken to ensure complete O_2 removal from the samples. The atmosphere inside the anoxic chamber (Coy Laboratories, Inc.) used in the study was maintained at a 96:4 mixture of N_2:H_2 gases that was continuously cycled through a Pd catalyst to remove traces of oxygen. A Model 10 gas monitor (Coy Laboratories, Inc.) indicated 0 ± 1 ppm O_2 content in the chamber atmosphere at all times. All vessels, bottles, pipette tips, flasks, etc., were equilibrated for several days inside the anoxic atmosphere before use. The dissolved O_2 content in the samples and titrants was checked before and after all experiments by using a CHEMets® colorimetric analysis kit R-7540 (2.5 ppb sensitivity). Solutions were used only if they tested negative for O_2. Others have demonstrated decreased Fe^{II} concentration with time in solutions left open in the anoxic chamber (Jeon et al., 2004). Removal of Fe^{II} was attributed to oxidation by residual O_2 in the chamber atmosphere (i.e., O_2 not removed by the Pd scrubber), with an estimated half-time of 10 days. In our study, the experiments were completed within 2 h after opening of the purged bottles in the anoxic chamber and placement of the suspensions in a closed reaction vessel.

Complexation of U^{VI} by dissolved carbonate ligands significantly affects U speciation. To exclude this competing process from our experiments, dissolved CO_2 was removed from the solutions by bubbling with purified N_2 gas. After the sealed bottles were opened in the anoxic chamber, the samples were quickly transferred to the reaction vessel. The headspace was purged with gas from the anoxic chamber that had been passed through an Ascarite® column to remove CO_2. Cyclic acid-base titrations of blank water samples treated the same way as the samples showed no evidence of dissolved carbonate for at least 4 h after the bottles were opened.

2.3. Acid-base titration and metal uptake

Titrations were carried out inside the anoxic chamber, using a computer-controlled TitraLab 90 titrator from Radiometer-Copenhagen. More information on the titrants, electrode, procedures, etc., can be found in the electronic annex. Samples for the XAFS experiments were brought to the desired pH by slow titration, transferred to 50-mL tubes (<1 mL headspace), and placed on an end-over-end rotator inside the anoxic chamber. A reaction time of 3 days was chosen on the basis of previous kinetic studies (Liger et al., 1999; Fredrickson et al., 2000; Jeon et al., 2005) and to allow time for possible mineral formation and particle ripening. Identical results were obtained in control samples after 4-months of reaction time. The solid and solution phases were separated in the anoxic atmosphere by filtration through a 0.22-μm membrane. The supernatants were acidified and brought out of the chamber for total Fe and U analysis with a Perkin-Elmer inductively coupled plasma-atomic emission spectrometer (ICP-AES) calibrated with matrix-matched standards. The estimated detection limits are 2 ppb for Fe and 15 ppb for U. To minimize experimental artifacts, 0.1 mM Y was added as an internal standard to all samples and standards. Measurements were made in triplicate, and the average and standard deviation were used. The Fe^{II} concentration was measured by using the ferrozine method (Sørensen, 1982).

2.4. X-ray absorption experiments/standards

The Fe K-edge and U L_{III}-edge XAFS experiments were carried out at the Materials Research Collaborative Access Team (MRCAT) beamline, sector 10 at the Advanced Photon Source (Segre et al., 2000). The beamline undulator was tapered, and the incident energy was scanned by using the Si(111) reflection of the double-crystal monochromator in quick-scanning mode (approximately 2 min per scan for the extended region and 30 s per scan for the near-edge region). More details on the XAFS data collection and analysis procedures can be found in the electronic annex.

The filtered wet paste samples were mounted in drilled Plexiglas slides and sealed with Kapton film windows inside the anoxic chamber. Separate tests showed that sealed slides left in the air kept the sample inside anoxic for at least 8 h. In our experiments, the sealed slides were exposed to air for about 1 min while being transferred from an O_2-free container to the N_2-purged detector housing. All samples were handled identically.

Several solution and polycrystalline samples were used as XAFS standards in the analysis. Acidic (pH 2–3) solutions of ferrous and uranyl chloride were used as standards for the structure of hydrated Fe^{II} and U^{VI}. The structure of aqueous Me–acetate complexes (Me = Fe^{II}, U^{VI}) were used as analogues of the Me–carboxyl complex at the surface. For an aqueous Fe^{II}–acetate (Fe^{II}–Ac) complex, a solution of composition $[Fe^{II}] = 60$ mM, [Na–Ac] = 2 M, pH 6.1 [speciation: 90% $FeAc_2$, 8% FeAc, 2% Fe(aq)] was used. For an aqueous U^{VI}–Ac complex, a solution of composition $[U^{VI}] = 1$ mM, [Na–Ac] = 100 mM, pH 5.5 (speciation: 100% UAc_3) was used. The EXAFS amplitudes and phases calculated by FEFF were calibrated by using data from fine-powder standards of known Fe and U crystal structures, mounted on tape and measured in transmission mode or diluted in SiO_2 and measured in fluorescence mode. The powder uraninite ($U^{IV}O_2$) standard was purchased from Alfa Aesar and diluted 1:100 in SiO_2. X-ray diffraction indicated ~95% purity (Kelly et al., 2002).

3. RESULTS

3.1. Acid-base titrations

Fig. 1 shows added $[OH^-]$ vs. pH obtained by titration of the experimental systems with NaOH. Vertical differences between the unbuffered electrolyte curve (open up-triangles) and all other curves are indicative of OH^- consumption in reactions such as hydrolysis or precipitation of solvated metals, or in the formation of water with the H^+ released from proton-active surface groups. The behavior of the isolated components (colloid, Fe, U) will be discussed first, followed by the binary (colloid + Fe, colloid + U), and ternary (colloid + Fe + U) systems.

For the carboxyl-modified colloid suspension, the release of adsorbed H^+ starts at about pH 5.0 and continues throughout the pH range (solid triangles). The titration curve is significantly different from that of a monofunctional carboxylic acid in solution. Deprotonation starts at higher pH values in the colloid and is completed over a broader pH range. Such pH shift and broadening can be simulated for carboxyl groups ($pK_a \sim 4$) by surface electrostatic effects and by heterogeneity in the carboxyl ionization constant, both resulting from the carboxyl groups being confined to the surface. Indeed, titration curves showed a dependence on the background electrolyte concentration that indicates the presence of surface electrostatic effects. Analysis of the extended data set through use of double-layer models will be the subject of an upcoming report; for the purposes of this study, only titrations at 0.03 M ionic strength will be considered. The H^+ sorption capacity of the 4.2 g/L suspensions was calculated as 0.4 mM. For the homogeneous 1 mM $FeCl_2$ solution (Fig. 1, diagonal cross), the titration curve is consistent with that observed previously for Fe^{II} solutions (Arden, 1950; Doelsch et al., 2002). An interval of little or no OH^- consumption up to about pH 8.6 is followed by a vertical section with no pH change until the dissolved Fe^{II} pool is consumed, presumably in $Fe(OH)_2$ precipitate formation. No significant Fe^{III} appears to be present in the solution, in view of the absence of an additional step in the titration curve in the pH 5–7 range that would result from mixed Fe^{II}–Fe^{III} mineral formation (Arden, 1950). For 0.1 mM solutions of U^{VI}, the titration curve follows the electrolyte curve up to about pH 4.5, indicating the presence of only UO_2^{2+}(aq) species. Subsequent steps were observed at higher pH, consistent with the formation of the U^{VI} hydrolysis complexes, such as UO_2OH^+, $UO_2(OH)_2^0$, $(UO_2)_3(OH)_5^+$, and $(UO_2)_4(OH)_7^+$, and precipitates (Grenthe et al., 1992).

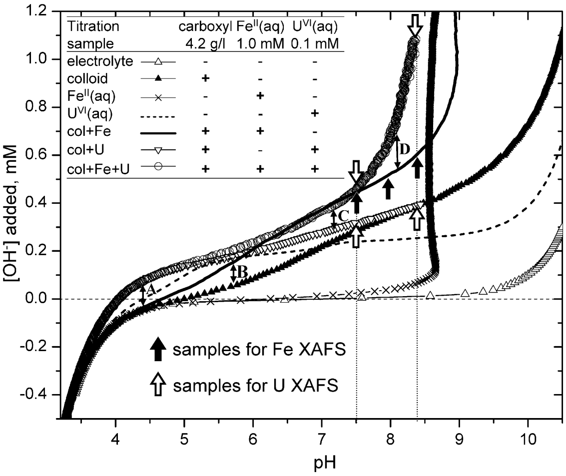

Fig. 1. Titration of acidified samples with 0.02 M NaOH. Double arrows (labeled A–D) point to differences in buffering capacity between samples that are discussed in the text. Block arrows show pH values at which filtered samples were prepared for XAFS analysis. The vertical dashed lines indicate the pH values at which XAFS spectra are compared. The table on the inset shows the composition of the titrated systems.

Titrations of the binary system colloid + Fe show increased OH^- consumption with pH relative to the colloid-only system (arrow B in Fig. 1). The OH^- consumption ratio between the two systems decreases from 3 at pH 5.5 until it levels off to 1.5 at pH 8.0, above which it increases again. Below a pH of approximately 7.5, the solvated Fe^{II} does not hydrolyze to a significant extent, so the additional buffering capacity observed in the binary colloid + Fe system is likely due to interactions between Fe^{II} and the colloid surface, such as proton release from the surface caused by Fe^{II} adsorption and/or hydroxylation of the adsorbed Fe^{II} (i.e., the formation of surface-$Fe^{II}(OH)_n$ species). Both adsorption and hydroxylation are consistent with specific (inner-sphere) binding of Fe^{II} to the carboxyl. Non-specific binding is unlikely to result in such a large increase in proton release, and hydroxylation of the otherwise hydroxylation-inert $Fe^{II}(aq)$ at low pH is unlikely to occur unless a bound ligand from adsorption facilitates the loss of H^+ on the opposite side of the metal (a *trans* ligand effect). For the binary system colloid + U (down-triangles in Fig. 1), increased OH^- consumption relative to the colloid-only and U^{VI}-only systems begins in the pH range 3.5–5.0 (arrow A). The enhanced OH^- consumption suggests surface H^+ release caused by specific U^{VI} sorption onto the colloid surface. Because this pH range is mostly below that of aqueous U^{VI} hydrolysis, the sorbed species are likely non-hydrolyzed $PS - COO^- - UO_2{}^{2+} \cdot nH_2O$, where PS is the polystyrene group to which the surface COOH is attached. No hydrolysis steps are seen at higher pH in the titration curve, in contrast to titrations of aqueous U^{VI}, suggesting that the adsorbed U^{VI} ions do not hydrolyze or form oligomers as they do in the absence of the surface.

The titration curve of the ternary system, colloid + Fe + U, displays features from both the colloid + U and the colloid + Fe systems (open circles in Fig. 1). For pH values between 3.5 and 5.3 the curve follows that of the colloid + U system, indicating U sorption to the surface. At higher pH the slope of the curve increases relative to that of the colloid + U system, and for pH values between 6.2 and 7.5 the curve follows that of the colloid + Fe system (arrow C). The additional OH^- consumption relative to the colloid + U system in this pH region can be interpreted as resulting from proton release due to Fe^{II} sorption. The convergence of the colloid + Fe + U titration curve first with the colloid + U curve and then with the colloid + Fe curve is consistent with competitive adsorption of U, Fe, and H to a limited number of discrete sites, implying specific binding rather than non-specific electrostatic adsorption to a distributed surface charge. Between pH 7.5 and pH 8.4, the slope of the titration curve increases dramatically relative to that of the colloid + Fe (arrow D). The slope is much larger than that of the sum of the colloid + U and the colloid + Fe systems, and therefore the increased OH^- consumption is the result of some interaction between Fe and U at the surface. A likely cause for the steep increase is the onset of a mineral-forming reaction, in addition to the surface-proton release and hydrolysis reactions that may be going on. Speculating at this point that a U^{VI}–Fe^{II} redox reaction is taking place, the formation of U^{IV} and Fe^{III} species will almost immediately exceed the solubility limit of U^{IV}- and Fe^{III}-containing minerals at this pH. We note that the reaction taking place above pH 7.5 occurs on the time scale of minutes, as the entire titration is completed within an hour.

3.2. XAFS spectroscopy

Suspensions of the binary (colloid + Fe and colloid + U) and the ternary (colloid + Fe + U) systems were prepared at pH values shown by block arrows in Fig. 1. All colloid + U and colloid + Fe samples, as well as the colloid + Fe + U sample at pH 7.5, had the same white color as did the acidified suspensions. Some flocculation of the suspension was observed in the colloid + Fe sample at pH 8.4. In contrast, the colloid + Fe + U suspension at pH 8.4 settled quickly and had a distinct gray-brown color (Fig. EA-2 in the electronic annex). The suspensions were filtered, and the supernatants were analyzed for total Fe and U content. The results are summarized in Table 2. The 0.1 mM uranium was removed from solution in all samples, whereas the 1.0 mM iron was partitioned between the solid and solution phases. The amounts of both adsorbed and solvated Fe^{II} were sufficient for stoichiometric reduction of 0.1 mM U^{VI} in all 4.2 g/L samples (i.e., >0.2 mM). Two control samples, colloid + Fe + U at pH 7.5 and pH 8.4, were sealed and filtered after 4 months in the anoxic atmosphere.

The hydrated solid phases were analyzed by Fe K-edge and U L_{III}-edge XAFS spectroscopy, which probed the valence and atomic structure of the adsorbed species. Control measurements showed that a 1 mM Fe^{II} solution produced a negligible absorption signal relative to the one measured in the wet pastes, so spectral contributions from Fe^{II} remaining in the pore water of the pastes can be neglected. The quality of the measured EXAFS data is illustrated in Fig. EA-3 in the electronic annex.

3.2.1. Fe K-edge XANES and EXAFS analysis

XANES measurements on the colloid + Fe pastes confirmed that the adsorbed Fe atoms were in the +2 valence state (Fig. EA-4 in the electronic annex). Fourier transforms (FT) of the EXAFS data are compared to standards in Fig. 2. Interpretation of the spectra is based on the coordination environment of Fe^{II} in crystal oxides/hydroxides

Table 2
Total Fe and U concentrations in the supernatants of the samples filtered for the XAFS experiments, $[Me]_{sol}$, determined by ICP-AES

Sample	pH	[colloid] (g/L)	$[U]_{sol}$ (mM)	$[U]_{ads}$ (mM)	$[Fe]_{sol}$ (mM)	$[Fe]_{ads}$ (mM)	U (Å^2/atom)	Fe (Å^2/atom)
Colloid + Fe	7.5	4.2	—	—	0.71	0.29	—	14.8
Colloid + Fe	8.4	4.2	—	—	0.55	0.45	—	9.5
Colloid + U	7.5	4.2	0.00	0.10	—	—	42.9	—
Colloid + U	8.4	4.2	0.00	0.10	—	—	42.9	—
Colloid + Fe + U	7.5	4.2	0.00	0.10	0.72	0.28	42.9	15.3
Colloid + Fe + U	8.4	4.2	0.00	0.10	0.31	0.69	42.9	6.2
Colloid + Fe + U	7.5	20.0	0.00	0.10	0.19	0.81	204.3	25.2
Colloid + Fe + U	8.4	20.0	0.00	0.10	0.09	0.91	204.3	22.5

Metal uptake, $[Me]_{ads}$, and calculated area per adsorbed metal atom are determined from $[Me]_{sol}$. The calculated H^+ sorption capacity of 4.2 g/L colloid suspensions is 0.4 mM. Standard deviations in concentration values are less than the accuracy shown.

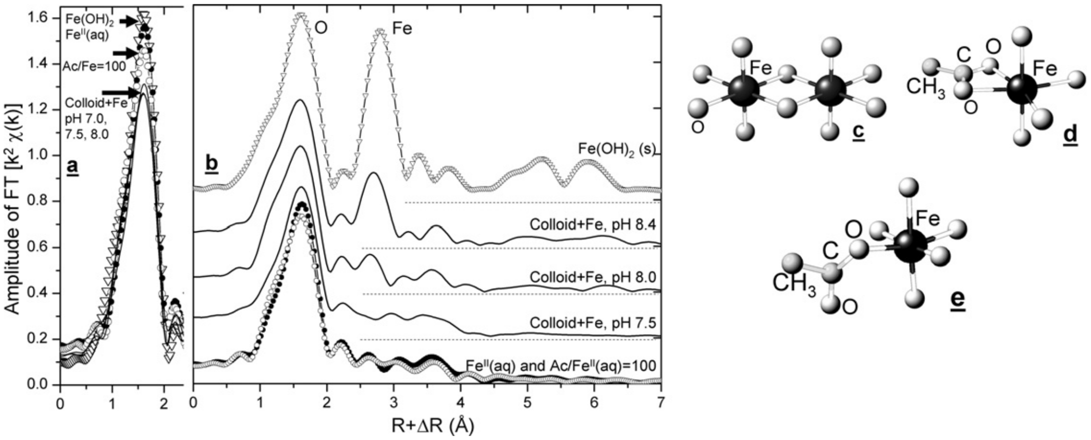

Fig. 2. Fourier transform of Fe K-edge EXAFS data (k^2-weighed, $\Delta k = 2.4$–10.5 Å^{-1} with a 1 Å^{-1} Hanning window). (a) Comparison of O-shell peak amplitude. The line convention is the same as in (b). Arrows indicate the peak heights of the samples listed to the left of the arrows. (b) Comparison between colloid + Fe samples and standards. Spectra are offset vertically for clarity. (c) Bond geometry between Fe atoms in $Fe(OH)_2$. (d) Bidentate binding mode of an acetate group to a metal atom. Both O atoms of the carboxyl group are involved in the bond. (e) Monodentate binding mode of an acetate group to a metal atom. Only one of the carboxyl O atoms participates in the bond.

and in solution. In crystalline $Fe(OH)_2$, Fe^{II}–O_6 octahedra (six O atoms at 2.15 Å) share edges (Fig. 2c) and form layered sheets, resulting in sixfold Fe–Fe coordination at 3.26 Å in each layer (Lutz et al., 1994; Doelsch et al., 2002). The O shell is reflected in the single FT peak at around 1.6 Å, and the sixfold Fe–Fe coordination is reflected in the single FT peak around 2.8 Å in the $Fe(OH)_2$ standard spectrum. The three data sets for Fe^{II} sorbed to the carboxyl colloid have the smallest amplitude of the 1.6 Å peak (Fig. 2a). Modeling of the Fe EXAFS data is given in Fig. EA-5 in the electronic annex. It indicates a broader distribution of Fe–O distances (larger Debye–Waller factor) relative to that in the solution standards and is consistent with replacement of hydration water molecule(s) by ligand oxygen atom(s). Comparisons of the FT structure at 1.9–2.3 Å between the colloid + Fe, the Fe^{II}–acetate standard, and the hydrated Fe^{II} standard show no evidence of a C atom signal in any of the spectra. A bidentate metal–carboxyl complex (Fig. 2d) typically produces a feature in that region due to coherent backscattering from the C atom, as in the cases of Cd^{II} and U^{VI} (Kelly et al., 2002; Boyanov et al., 2003). Conversely, no C atom feature is seen in spectra from a monodentate (Fig. 2e) Cu^{II}–acetate complex (Boyanov, 2003), likely because of loss of C backscattering coherence due to vibrations in this more flexible complex type. In the case of the colloid + Fe system, the lack of C signal, together with the indication of inner-sphere complexation from both the titration and the first-shell EXAFS data, strongly suggest a monodentate Fe^{II}–carboxyl complex as the adsorption mechanism. The FT data at 2.8 Å in the colloid + Fe spectra show no evidence of Fe–Fe coordination at pH 7.5, whereas increasing Fe–Fe coordination is seen at pH 8.0 and 8.4. The average Fe^{II}–Fe^{II} coordination of 3 ± 1 atoms obtained by fitting the pH 8.4 spectrum is lower than in bulk $Fe(OH)_2$; this can be explained either if about 50% of the Fe atoms in the sample are in a bulk precipitate and the rest are adsorbed as monomeric atoms, or by undercoordination of the surface Fe atoms in nanometer-sized $Fe(OH)_2$ particles that are attached to the polystyrene microspheres. Fits of the EXAFS data indicate strain in the Fe–O bonds, which suggests that a bulk $Fe(OH)_2$ precipitate is not formed (Fig. EA-5 in the electronic annex shows contraction of the distances and larger Debye–Waller factors in the pH 8.4 system relative to the $Fe(OH)_2$ standard). Regardless of the form of the phase with Fe–Fe coordination, the EXAFS data establish the presence of oligomeric edge-sharing Fe^{II} octahedra in the solid phase at pH 8.4 (schematic bond structure shown on Fig. 2c), whereas only monomeric species are present at pH 7.5. "Oligomeric" here is used in the sense of "having local Fe^{II}–Fe^{II} coordination", which can include Fe dimers, polymers, or bulk precipitate.

3.2.2. U L_{III}-edge XANES analysis

Fig. 3 compares U XANES data from the colloid + U and colloid + Fe + U systems to standards. A higher energy position of the absorption edge and a shoulder at 17,190 eV are indicative of U in the +6 valence state and the UO_2^{2+} (uranyl) coordination geometry (Hudson et al., 1995; O'Loughlin et al., 2003). A lower energy position of the edge, lack of the shoulder at 17,190 eV, and higher amplitude of the peak immediately after the edge indicate U in the +4 valence state. The XANES data verify the predominantly U^{VI} state and uranyl geometry in the colloid + U system (within the experimental uncertainty). In the ternary colloid + Fe + U system, U is present predominantly as U^{VI} at pH 7.5 and predominantly as U^{IV} at pH 8.4. The same results were obtained for the pH 7.5 and pH 8.4 samples that were left for 4 months in the anoxic atmosphere. Typical accuracy of valence state determinations from XANES data is about 10–15%.

3.2.3. U^{VI} EXAFS analysis

Fig. 4 compares EXAFS data from the three U^{VI} samples to data from two aqueous standards: a hydrated and an acetate bound U^{VI}. The magnitude of the FT between

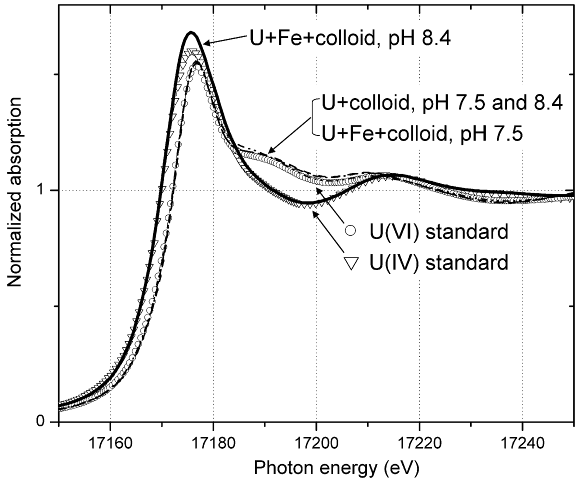

Fig. 3. Normalized uranium L_{III}-edge XANES spectra from the colloid + U (+Fe) samples compared to a U^{VI} and U^{IV} standard. An edge position at higher energy and a shoulder at 17,190 eV indicates U^{VI}, whereas an edge position at lower energy and lack of the shoulder indicate U^{IV}.

1.0 and 2.2 Å displays the splitting of the O near-neighbors in an axial and an equatorial shell, characteristic of the uranyl geometry. Two axial O atoms at about 1.75 Å and 4–6 equatorial O atoms at larger distance, usually 2.3–2.5 Å, are seen in many U^{VI} compounds (Morosin, 1978; Templeton et al., 1985; Fischer, 2003; Kubatko and Burns, 2004). The axial atoms are inert to chemical substitution, so complexation occurs in the equatorial plane. A comparison between the hydrated and acetate-bound U^{VI} standards shows the effect of substituting equatorial water molecules with a carboxyl ligand (vertical lines on Fig. 4). The feature of interest is better seen in the real part of the FT (inset). The acetate-bound U^{VI} standard (triangles) shows an oscillation centered at around 2.4 Å relative to the hydrated U^{VI} (circles). Modeling shows that this feature is due to C atom(s) in a bidentate geometry (Fig. EA-6 in the electronic annex), consistent with previous work (Kelly et al., 2002). Therefore, U^{VI} is adsorbed to the carboxyl colloid as a bidentate carboxyl complex. The C signal amplitude in the adsorbed U spectra is smaller than that in the U^{VI}-acetate standard (speciation 100% $[UO_2Ac_3]$), suggesting a 1:1 or 1:2 U^{VI}:acetate stoichiometry. Exact stoichiometry assignment is problematic, given the dependence of EXAFS amplitudes on both coordination number and Debye–Waller factor (related to the bond strength), and the unknown, likely inverse relation between bond strength and bond number. No evidence of a U near-neighbor is observed in any of the three spectra, indicating lack of significant U oligomerization between the adsorbed U^{VI} atoms. There is also no evidence of an Fe backscatterer in the colloid + Fe + U spectrum at pH 7.5, indicating lack of bonds between the adsorbed Fe^{II} and U^{VI} atoms in the ternary system. The colloid + U samples at both pH 7.5 and pH 8.4 have nearly identical spectra, indicating that no change in adsorbed U^{VI} speciation occurs over this pH range.

3.2.4. U^{IV} EXAFS analysis

Fig. 5 compares data for the colloid + Fe + U system at pH 8.4 to data for a U^{IV} standard, a UO_2 (uraninite) mineral. The features of the FT magnitude are similar to those of the uraninite standard, but the amplitudes of the peaks in the colloid + Fe + U spectrum are significantly smaller. The peak at 1.8 Å is due to the cubical O shell in UO_2, whereas the double peak between 2.9 and 4.5 Å is mostly due to the 12-member U shell at $R = 3.87$ Å in UO_2, the splitting coming from the characteristic backscattering amplitude of U. Modeling of the data shows that the

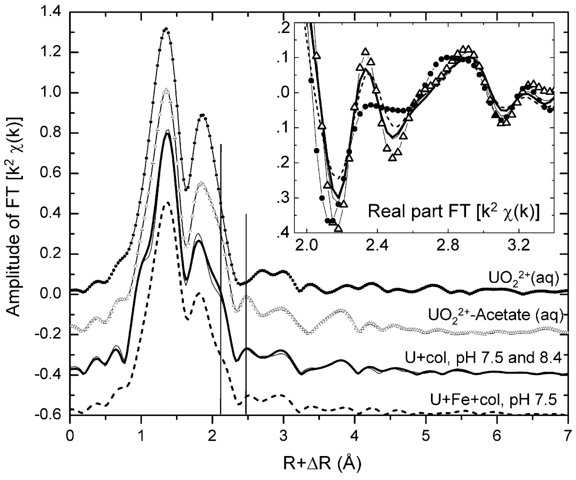

Fig. 4. Fourier transform of U L-edge EXAFS data from U^{VI} samples and standards (k^2-weighed, $\Delta k = 2.8$–13.5 Å^{-1} with a 1 Å^{-1} Hanning window). Vertical lines indicate the positions of features resulting from the C shell contribution in the EXAFS data. Inset: Real part of the FT in a smaller R-range. The line convention is the same as for the magnitude of FT.

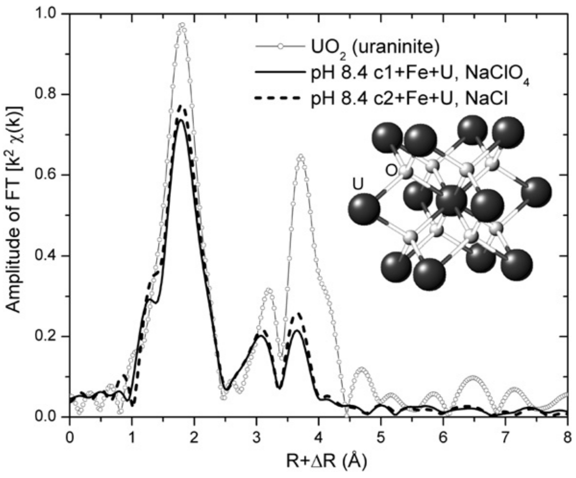

Fig. 5. Fourier transform of U L-edge EXAFS data for U^{IV} samples and standards (k^2-weighed, $\Delta k = 2.2$–10.4 Å^{-1} with a 1 Å^{-1} Hanning window). The dashed line shows the repeatability of the spectrum with a different electrolyte and a different batch of adsorbent, measured during a different beamline experiment. The crystal structure of uraninite, UO_2, is illustrated in the inset.

smaller amplitude of the 1.8 Å peak is due to a larger Debye–Waller factor (Table 3A and B), indicating a broader U–O bond length distribution in the colloid + Fe + U sample than in the UO_2 standard. When modeled with a single U shell, the smaller doublet amplitude in the colloid + Fe + U data at pH 8.4 can be attributed to smaller average U–U coordination and larger disorder in that shell relative to the standard (Table 3A and B). The drop in average coordination number from 12 in crystalline UO_2 to 6.9 ± 2.7 in the colloid + Fe + U pH 8.4 system can be attributed to either partitioning of the U^{IV} between a monomeric phase and a precipitate, or formation of nanometer-sized uraninite particles. In the latter, more likely case, we estimate the average particle size to be less than 3.5 nm in diameter (Fig. EA-7 in the electronic annex). The presence of U^{IV} in nanoparticulate form may also be the reason why the structure between 3 and 4.5 Å (Fig. 5) appears simpler in the pH 8.4 sample than in the uraninite standard. Disorder caused by strain in a small particle is likely to reduce the spectral contribution of multiple-scattering and outer-shell paths significantly more than that of single-scattering paths, resulting in mostly single-scattering content in the pH 8.4 spectrum.

Further analysis of the doublet between 3 and 4 Å in Fig. 5 reveals that the peak amplitudes are in about 1:2 ratio for the UO_2 standard, whereas that ratio is about 1:1 in the pH 8.4 sample. Equal ratios are expected in the two spectra if the amplitude difference between the sample and standard is due to the difference in U–U coordination only. The reason for this different amplitude ratio was

Table 3
Results from modeling of the U^{IV} EXAFS data[a]

Shell	N	R (Å)	σ^2 (10^{-3} Å^2)[b]	ΔE_0(eV)	Fit quality[c]
(A) UO_2 standard					
O→	8.0	2.37 ± 0.01	6.7 ± 2.1	−2.1 ± 0.8	208
MS→	8.0	4.73 ± 0.02	13.4 ± 4.2	−2.1 ± 0.8	0.037
O2→	24.0	4.54 ± 0.04	16.6 ± 8.6	−2.1 ± 0.8	9
U→	12.0	3.88 ± 0.01	4.4 ± 1.2	−2.1 ± 0.8	
(B) U + Fe + colloid, pH 8.4, full *R*-range					
O→	7.9 ± 0.6	2.36 ± 0.01	10.9 ± 1.7	−0.7 ± 0.6	241
MS→	7.9 ± 0.6	4.73 ± 0.02	21.8 ± 3.4	−0.7 ± 0.6	0.016
O2 →	24.0	4.43 ± 0.09	48.9 ± 16.6	−0.7 ± 0.6	8
U→	6.9 ± 2.7	3.84 ± 0.02	9.1 ± 3.3	−0.7 ± 0.6	
(C) U + Fe + colloid, pH 8.4, limited *R*-range					
O→	7.9	2.36	10.9	−0.7	190
MS→	7.9	4.73	21.8	−0.7	0.047
O2→	24.0	4.42 ± 0.07	51 ± 13	−0.7	5
U→	6.5 ± 2.3	3.85 ± 0.02	8.7 ± 3.0	−0.7	
(D) U + Fe + colloid, pH 8.4, limited *R*-range, unconstrained Fe					
O→	7.9	2.36	10.9	−0.7	60
MS→	7.9	4.73	21.8	−0.7	0.006
O2→	24.0	4.47 ± 0.04	39.8 ± 10.0	−0.7	2
U→	8.5 ± 2.1	3.85 ± 0.01	10.7 ± 1.9	−0.7	
Fe→	4.2 ± 4.5	3.56 ± 0.03	21.4 ± 13.3	−0.7	
(E) U + Fe + colloid, pH 8.4, limited *R*-range, constrained Fe					
O→	7.9	2.36	10.9	−0.7	61
MS→	7.9	4.73	21.8	−0.7	0.009
O2→	24.0	4.46 ± 0.04	45.5 ± 7.2	−0.7	3
U→	8.1 ± 1.8	3.85 ± 0.01	11.1 ± 2.0	−0.7	
Fe→	1.5 ± 0.4	3.56 ± 0.02	10.0	−0.7	

(A) Fit of the uraninite (UO_2) standard data in the range $R + \Delta R = 1.41$–4.35 Å.
(B) Fit of the U + Fe + colloid data in the range $R + \Delta R = 1.41$–4.35 Å using the uraninite model.
(C) Fit of the U + Fe + colloid data in the range $R + \Delta R = 2.82$–4.35 Å using the uraninite model with fixed first-shell parameters.
(D) Fit of the U + Fe + colloid data in the range $R + \Delta R = 2.82$–4.35 Å using the uraninite model with an added Fe shell.
(E) Fit of the U + Fe + colloid data in the range $R + \Delta R = 2.82$–4.35 Å using the UO_2 + Fe shell model with constrained Debye–Waller factor.

[a] Parameters for which uncertainties are not given are held constant during the fit. Uncertainties are estimated by the FEFFIT program. A single ΔE_0 parameter was refined for all shells. Multiple-scattering (MS) parameters for the O shell were constrained to those for the single-scattering paths, assuming uncorrelated thermal motion in the O shell ($N_{MS} = N_O$, $R_{MS} = 2R_O$, and $\sigma^2_{MS} = 2\sigma^2_O$).

[b] Disorder parameter (EXAFS Debye–Waller factor).

[c] Given from top to bottom for each fit are χ^2_v (goodness-of-fit indicator taking into account the number of data points and variables used), *R*-factor (the fractional misfit: difference between data and model relative to the absolute value of the data), and degrees of freedom in the fit (number of independent points minus number of variables). More information on these parameters is given in the FEFFIT documentation (see Section 2.2).

determined by simultaneously fitting the k^1, k^2, and k^3 weighted EXAFS spectra with the same set of parameters (Kelly et al., 2002; Haskel et al., 2004). The detailed analytical procedure is given in the electronic annex. Modeling of the uraninite standard data at k^1, k^2, and k^3 weights is shown at the top of Fig. 6a. The uraninite model reproduces well the features of the data simultaneously at all k^n weights with parameters given in Table 3A. The same model, when applied to the reduced uranium data from the colloid + Fe + U system at pH 8.4, is unable to reproduce the amplitude ratio and features in the U doublet at all three k^n-weights (Fig. 6b and Table 3B). The addition of a third or fourth cumulant disorder parameter to the U shell also did not improve the fit. All of the above suggests the presence of a spectral contribution around 3.1 Å in the pH 8.4 system that is not present in the uraninite standard.

The best fit of the data was obtained by adding an Fe shell at 3.56 Å to the model used for the uraninite standard. Details on why this model was chosen and how it compensates the misfit at all three k^n FT weights are given in the electronic annex. The quality of the fit is shown in Fig. 6c, and the parameters from an unconstrained Fe-shell fit are given in Table 3D. The strong correlation between the coordination number and Debye–Waller (σ^2) of the Fe shell was removed by assuming a σ^2 of 0.010 Å^2 for the Fe shell (similar to that obtained for the O shell), and a constrained fit produced the parameters in Table 3E. Applying a range of reasonable constraints for the Debye–Waller factor (0.005–0.015 Å^2) yielded a coordination number between 1 and 2 Fe atoms around each U^{IV} atom.

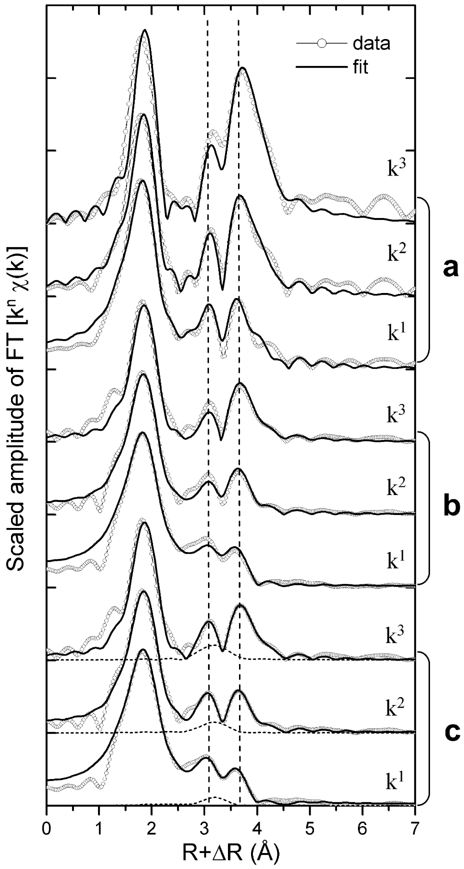

Fig. 6. FEFF8/FEFFIT modeling of data from U^{IV} samples. Fourier-transformed $k^n\chi(k)$ data are scaled as follows: $k^3 \times 1$, $k^2 \times 5$, $k^1 \times 23$. Fit parameters are given in Table 3. Vertical dashed lines indicate the peak positions of the U doublet. (a) UO_2 data modeled with the O + U shell model, (b) colloid + Fe + U sample at pH 8.4 modeled with the O + U shell model, (c) colloid + Fe + U sample at pH 8.4 modeled with the O + U + Fe shell model. The contribution from the Fe atoms is given by the dashed peaks.

An edge-sharing U^{IV}–Fe complex geometry is compared to the uraninite U^{IV}–U^{IV} coordination geometry in Fig. 7. Assuming that the U–O bond geometry is not affected by the Fe atom, we calculated an Fe–O distance of 2.12 Å and an O–Fe–O angle of 80 deg from the observed U–Fe distance. Some adjustment of the bond angles can be expected in a U–Fe complex, leading to slightly shorter or longer Fe–O distances. The geometrically derived Fe–O distance and O–Fe–O angle are consistent with Fe octahedra found in Fe^{II} compounds [2.15 Å in FeO, $Fe(OH)_2$, and $FeCO_3$], Fe^{III} oxides/hydroxides [1.95–2.09 Å in hematite, goethite, lepidocrocite], and magnetite [2.06 Å for octahedral Fe^{II} or Fe^{III}] (Wyckoff, 1960; Blake et al., 1966; Forsyth et al., 1968; Christensen et al., 1982; Wechsler et al., 1984; Lutz et al., 1994).

The spectrum of the colloid + Fe + U pH 8.4 sample, showing smaller U^{IV}–U^{IV} coordination and Fe in the local U^{IV} environment, could be the result of two possible scenarios. If all U^{IV} is in a single phase, the observed average local environment can be achieved in the structure shown in Fig. EA-8 in the electronic annex. This structure can be described as an Fe-coated uraninite plate, in which an interface between oligomeric U^{IV} and Fe species produces the U–Fe and U–U coordination observed by EXAFS. Alternatively, U^{IV} may be partitioned between two phases: U^{IV} in uraninite particles and monomeric U^{IV} adsorbed in an edge-sharing geometry to the $Fe^{II,III}$ oxide/hydroxide produced from Fe^{II} oxidation. This scenario seems less likely, because the amount of uranium in each of the latter phases needs to be comparable to produce the observed spectrum.

3.2.5. Fe XAFS analysis of the Colloid + Fe + U system

The colloid + Fe + U pH 8.4 sample was also analyzed by Fe XAFS to correlate U^{VI} reduction with Fe^{II} oxidation

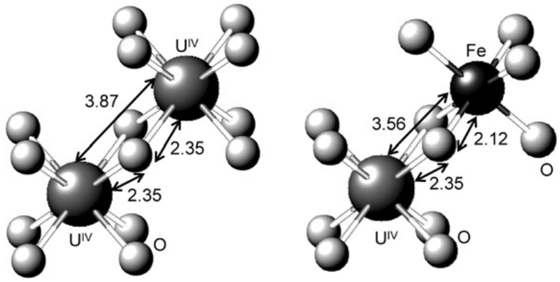

Fig. 7. Geometry of the U–U bond in uraninite (left), compared to the U–Fe coordination obtained in the colloid + Fe + U sample at pH 8.4 (right). The Fe–O bond distance and the O–Fe–O bond angle of 80 deg were calculated from the U–Fe bond distance.

and to characterize the resulting Fe phase. Interpretation of the data is problematic, because less than 30% of the Fe atoms present in the sample are expected to be oxidized. Table 2 shows that the 0.1 mM U was completely removed from solution and that total Fe in the solid phase was about 0.7 mM. Assuming that the oxidized Fe^{III} produced by stoichiometric reduction of U^{VI} was all present in the solid phase, the Fe^{III}/Fe^{II} ratio should be less than 30% (0.2/0.7). Fig. 8a compares the XANES data to Fe standards of valence state between +2 and +3. The edge position and shape of the pH 8.4 spectrum are consistent with an Fe^{III}/Fe^{II} ratio of 30% or less, and they show a higher Fe^{III}/Fe^{II} ratio at pH 8.4 than at pH 7.5. The higher Fe^{III} content, concurrent with U^{VI} reduction in the pH 8.4 sample, is evidence of the electron transfer from Fe^{II} to U^{VI} atoms.

Fig. 8b shows the Fe EXAFS data. Spectra from the colloid + Fe ± U samples at pH 7.5 are identical, indicating the same monomeric Fe^{II} species regardless of the presence of adsorbed U^{VI}. In contrast, the spectrum of the colloid + Fe + U pH 8.4 sample shows peaks between 2.3 and 3.5 Å that are likely due to adjacent Fe atoms in an iron mineral structure or structures. As already discussed, interpretation of data from this sample is complicated by the presence of mixed Fe^{II}/Fe^{III} species. Comparison to the spectra of standards that are representative of the possible end phases (Fe^{II}, Fe^{III}, and mixed-valence minerals, e.g., $Fe(OH)_2$, green rust, magnetite, goethite, hematite, etc.) shows that the second-shell structure is most similar to that of magnetite. Magnetite is a common product of Fe^{II} oxidation in bacterial and abiotic systems at circumneutral pH (Cornell and Schwertman, 1996; Chaudhuri et al., 2001) and can therefore be anticipated in the pH 8.4 system as well. The reduced O and Fe peak amplitudes relative to the standard are consistent with partitioning of the Fe between magnetite and adsorbed Fe^{II}.

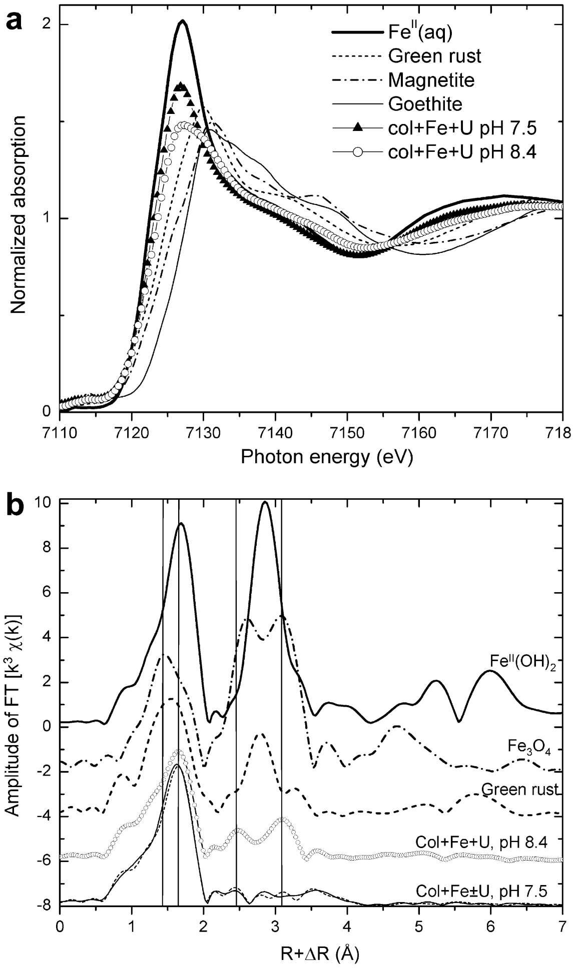

Fig. 8. Fe K-edge data from colloid + Fe + U samples compared to standards. (a) XANES, (b) FT of EXAFS. The similar FT magnitudes of spectra from samples with and without U at pH 7.5 are shown at the bottom. Vertical lines indicate the similarity of EXAFS features between the Fe + U + col sample at pH 8.4 and magnetite.

3.2.6. Effect of surface area and Fe^{II} concentration on U^{VI} reduction

Increasing the suspension concentration in the colloid + Fe + U system from 4.2 to 20 g/L while keeping the concentrations of U and Fe constant resulted in the removal of more Fe from the solution at both pH 7.5 and 8.4 (Table 2). The U XANES spectra of the samples at both pH 7.5 and 8.4 were identical to those of the colloid + U only system at 4.2 g/L loading (Fig. 3), indicating that U^{VI} reduction was not occurring in any of the 20-g/L samples after 3 days. The spectra of 4.2-g/L colloid + Fe + U samples at pH 8.4 in which the Fe^{II} concentration was reduced from 1.0 to 0.4 mM were also identical to those of the colloid + U system, indicating no significant U^{VI} reduction after 3 days. Fe K-edge EXAFS on the samples described above (increased surface area and decreased Fe concentration) showed no Fe–Fe coordination peaks in the spectra, indicating no Fe^{II} oligomerization under these conditions.

3.2.7. Reoxidation of the reduced U particles in air

Following a U XANES measurement of an anoxic colloid + Fe + U sample at pH 8.4 (~100% U^{IV}), the surface of the wet sample was exposed to air. No significant oxidation was seen within 15 min. After that, the U^{VI}/U^{IV} ratio increased at approximately 10% h^{-1} for the first 7 h. The next XANES measurement after 21 h of exposure to air showed 100% reoxidation to U^{VI}. These measurements show that the reduced U^{IV} product in the pH 8.4 colloid + Fe + U system is unstable to oxidation in air and provide an estimate of the rate of oxidation. They also serve as control experiments, showing that the anoxically sealed samples are not susceptible to possible oxidation during the measurement in a way that can be noticed in the XAFS spectra or analysis.

4. DISCUSSION

The combination of pH titrations, uptake measurements, and XAFS spectroscopy allows us to look for correlations between the reactivity and the speciation of the same system. Such correlations provide important insight and constrain our mechanistic interpretation of both adsorption and redox processes. When molecular information about speciation at a surface is unavailable, the tendency is to extrapolate bulk speciation to the surface. This may not be accurate if the electrostatic and steric contributions to the surface binding energy are significant, and may result in inaccurate interpretation of observed reactivity. The following results in our work underscore this point.

In studying the adsorption of Fe^{II} to the carboxyl surface, we observed additional OH^- consumption in the colloid + Fe system relative to the colloid by itself (Fig. 1, arrow B). Without knowledge of the molecular structure of the adsorbate, the OH^- balance can be explained by (1) carboxyl deprotonation due to changes in surface electrostatics caused by outer-sphere Fe^{II} adsorption, (2) deprotonation (H^+ displacement) caused by inner-sphere Fe^{II} adsorption, or (3) hydrolysis of the adsorbed Fe^{II} species. However, the relatively disordered O shell of the adsorbed Fe^{II} atoms observed by EXAFS, together with the significant OH^- consumption in titration experiments, suggests an inner-sphere complexation mechanism. This result is unexpected in view of the small binding affinity of Fe^{II} to carboxyl ligands [$\mathrm{Log}\,K = 0.54$, (Martell et al., 2001)]. Unfortunately, EXAFS cannot determine unequivocally whether the adsorbed Fe^{II} species are hydrolyzed. We speculate that the adsorbed Fe^{II} species are probably not hydrolyzed, because substitution of hydration molecule(s) for OH^- ligand(s), with the resulting charge neutralization of the adsorbed cation, is likely to lead to changes in the O shell larger than those observed by EXAFS. The reactivity implication of inner-sphere-adsorbed Fe^{II} is higher redox reactivity than a fully hydrated adsorbed species.

Another example of unexpected speciation is the observed Fe^{II} oligomerization in the colloid + Fe system at pH 8.0 and pH 8.4. The titration curve shows no significant change in slope between pH 7.5 and pH 8.4 (Fig. 1) and precipitation of the aqueous Fe^{II} phase in the system presumably occurs around pH 8.8 (vertical section). Fe^{II} uptake also does not conclusively establish precipitation, because uptake at pH 8.4 is about the same as the total surface site concentration (Table 2). Because of the large spread of $Fe(OH)_2(s)$ solubility constants in the literature ($\mathrm{Log}\,K_{sp}$ range from −13.1 to −15.3, Leussing and Kolthoff, 1953), we could not determine whether the Fe^{II}–Fe^{II} coordination is predicted from supersaturation of the solution phase at pH 8.4 or is the result of oligomerization of surface species at undersaturated conditions. The EXAFS results however provide unequivocal evidence of Fe^{II}–Fe^{II} coordination (i.e., Fe^{II} oligomerization) in the solid phase. Oligomerization implies the presence of hydrolyzed Fe^{II} species that combine to form oligomers. The reactivity implication from the presence of hydrolized/oligomerized Fe^{II} species is higher redox reactivity above pH 8.0.

Similarly for U^{VI} adsorbed to the carboxyl surface, the speciation observed in the colloid + U system appears different from that expected in bulk solution. A calculation for a solution containing no carbonate, 0.1 mM uranium, and 0.6 mM acetate, considering only hydrolysis and acetate-complexation reactions, showed that U^{VI} hydrolysis polymers should dominate the speciation at circumneutral pH and that U^{VI}–carboxyl complexes should exist only as a minor component between pH 4 and 5 (Fig. EA-9 in the electronic annex) (Grenthe et al., 1992; Martell et al., 2001). However, no hydrolysis steps were seen in pH titrations of the colloid + U system. The EXAFS data show that U hydrolysis oligomers are not present in the samples and that surface carboxyl complexation is responsible for the U uptake. The observations above suggest that surface complexation is responsible for the uptake throughout the pH range and that U^{VI}–carboxyl stability constants in the presence of a surface are significantly higher than those determined in bulk solution under the same conditions.

Our redox reactivity results show that monomeric adsorption of U^{VI} and Fe^{II} to the carboxyl surface (pH 7.5) does not lead to U^{VI} reduction over at least 4 months, despite sufficient surface and aqueous Fe^{II} concentrations for a stoichiometric reaction. These results suggest that both aqueous and carboxyl-adsorbed monomeric Fe^{II} species are not redox reactive toward U^{VI} under these conditions. Conversely, under conditions where Fe^{II} oligomers form in the colloid + Fe system (pH 8.4), complete and rapid reduction of U^{VI} occurs in the colloid + Fe + U system. EXAFS shows that speciation of the inner-sphere-adsorbed U^{VI} atoms does not change from pH 7.5 to pH 8.4 in the colloid + U system. Therefore, the increased reactivity at pH 8.4 relative to pH 7.5 is attributed to the difference in Fe^{II} speciation.

One possible mechanism for the increased Fe^{II} reactivity is a ligand effect. Binding to electron donor ligands (e.g., OH^- or CH_3COO^-) generally lowers the redox potential of reductant metals, presumably by increasing the electron density at the metal and facilitating the loss of electrons on the opposite side of the metal (Stumm, 1992; Sposito, 2004). Higher stability (i.e., lower energy) of an oxidized Fe^{III}–ligand complex relative to the reduced Fe^{II}–ligand complex may also provide a driving force for the electron transfer. Evidence for such effects are found in previous work: addition of carboxyl ligands increased the rate of Cr^{VI} and oxamyl reduction by Fe^{II} (Buerge and Hug, 1998; Strathmann and Stone, 2002); hydroxyl ligands were found to increase Fe^{II} reactivity towards O_2, Cr^{VI}, and organic pollutants (Sposito, 2004) (p.100 and references within). In the colloid + Fe + U system at pH 7.5, U^{VI} reduction is not enhanced by Fe^{II} complexation to the surface carboxyl, implying that a ligand effect is not sufficient to overcome the barrier to U^{VI} reduction. This implication does not preclude a ligand effect from hydroxylation, as the hydroxyl ligand might be a better electron donor than the carboxyl, or it might bridge between the Fe and U atoms. In kinetic measurements, the increased rate of U^{VI} removal in the presence of Fe^{II} and hematite was correlated to the amount of hydroxylated surface-adsorbed Fe^{II} species, $>Fe^{III}O\text{-}Fe^{II}OH^0$ (Liger et al., 1999). The surface hydroxylation hypothesis is also frequently used to explain increased reactivity of Fe^{II} in suspensions of metal oxides (e.g., Wehrli et al., 1989; Buerge and Hug, 1999; Strathmann and Stone, 2003; Elsner et al., 2004). However, the inherent uncertainty associated with surface speciation from titration data and the possibility of electron transfer through the oxide interface (Williams and Scherer, 2004) leaves other possibilities open. Our results from the increased-surface-area system at pH 8.4 (see Section 3.2.6) do not support surface species hydroxylation as the reason for enhanced reactivity in our system. The increase in the amount of adsorbed Fe^{II} at pH 8.4 with surface area (Table 2) should increase the amount of hydroxylated surface species present. The fact that we see complete U^{VI} reduction at low surface area and no reduction at high surface area suggests that (1) hydroxylated surface Fe^{II} species are not the species responsible for enhanced U^{VI} reduction, and (2) the actual reactive species are formed from the dissolved Fe^{II} species pool, which is decreased when the surface area is increased.

Exclusion of aqueous, carboxyl-adsorbed, and hydroxylated-adsorbed Fe^{II} species as the reactive species at pH 8.4 leaves aqueous $FeOH^+$ and oligomerized $Fe(OH)_2$-like species as possibilities (see Fig. 2c for the structure of the Fe–Fe bond in $Fe(OH)_2$). The Fe–Fe coordination observed at pH 8.4 in the low-surface-area system confirms the presence of the latter, but the former cannot be excluded. Although reactivity enhancement by OH^- ligands in $FeOH^+$ and $Fe(OH)_2$-like species appears to be a well-established mechanism (Sposito, 2004), the observed Fe–Fe coordination and the U^{VI} reduction occurring under the same conditions suggest another possible mechanism for increased Fe^{II} reactivity specifically toward U^{VI}: facilitation of the two-electron transfer by Fe^{II} oligomerization. Monomeric Fe^{II} can reduce oxidants that go through one-electron reduction steps (e.g., Cr^{VI}), so no obstacle for electron transfer from Fe^{II} to U^{VI} is apparent. Uranium is peculiar in that aqueous U^V rapidly disproportionates to U^{VI} and U^{IV} (Ekstrom, 1974). Thus, if aqueous U^V is the result of the one-electron transfer, then the reduction to U^{IV} should be completed through disproportionation. In the systems where reduction to U^{IV} does not occur, a bound U^V species must be formed. If the bound U^V species are stable, they will accumulate over time and be observable. We detected no U^V atoms by XAFS in the systems where reduction did not occur (colloid + Fe + U system at pH 7.5 or with increased surface area at pH 8.4), either by the edge position or by elongation of the axial U–O bond (Docrat et al., 1999). This result suggests that the hypothesized U^V–Fe^{III} intermediate is short-lived and experiences a quick electron back transfer to return to the original Fe^{II} and U^{VI} species. Such a non-productive pathway is known as a dead-end intermediate pathway (Haim, 1983). To complete the reduction to U^{IV}, a second electron needs to be transferred during the lifetime of the U^V intermediate. In aqueous solution with monomeric species, a three-body correlation between a U^{VI} and two Fe^{II} atoms is essentially required. The probability for this is exceedingly small; it likely provides the kinetic limitation to the U^{VI}–Fe^{II} reaction in solution. Conversely, if the Fe^{II} oligomer is already formed, a net two-electron transfer can occur more efficiently through the bonds between Fe^{II} atoms during the lifetime of the intermediate. Facilitation of a second electron transfer to a bound U^V species may also be the reason for the commonly observed high efficiency of U^{VI} reduction by Fe^{II} in the presence of oxide surfaces (Wersin et al., 1994; Liger et al., 1999; O'Loughlin et al., 2003; Ilton et al., 2004; Jeon et al., 2005). Adsorbed U^V species have been observed on dried mica surfaces by X-ray photoelectron spectroscopy (Ilton et al., 2005). Moderate stabilization of the U^V moiety by the surface is likely to provide greater opportunity for complete reduction to U^{IV}. Combined with possible electron transfer through the oxide (Williams and Scherer, 2004), the overall catalytic role of oxides may be to provide a second electron non-locally from adsorbed or structural Fe^{II} atoms to a stabilized U^V intermediate.

The proposed two-electron (non-disproportionation) mechanism for abiotic reduction of U^{VI} by Fe^{II} is in contrast to recent studies of enzymatic U^{VI} reduction by *Geobacter sulfurreducens* (Renshaw et al., 2005). The authors conclude that disproportionation of U^V is responsible for the second electron transfer step and that reduction goes through a stable (i.e., measurable by EXAFS) U^V intermediate. It is possible that the complexation and redox properties of enzymes are different than those of Fe^{II} and cause a different mechanism to occur in biological systems, one in which the transition from U^V to U^{IV} is the rate-limiting step. Conversely, because of the possibility for a quick two-electron transfer when Fe^{II} atoms are connected through bonds or a crystal, the rate-limiting step in these systems may be the initial complexation between the redox centers or the U^{VI} to U^V reduction. Observation of U^V species in this case will require a technique with better time resolution than XAFS.

As discussed in Section 3.2.4, we observed U^{IV}–Fe coordination in the colloid + Fe + U system at pH 8.4. This result provides support for the involvement of Fe^{II} in both reduction steps (as opposed to a disproportionation step from U^V to U^{IV}): if aqueous U^V disproportionation was responsible for the second reduction step, the resulting "free" U^{IV} atoms would likely bind to other U^{IV} atoms (because of the extremely low solubility of U^{IV} minerals), and the U^{IV}–Fe coordination would not be observed. The U^{IV}–Fe coordination suggests that the U and Fe atoms remain together in an inner-sphere complex after the first or both electron transfer steps.

The arguments presented above may provide insight into controls on the efficacy of abiotic U^{VI} reduction by surface-associated Fe^{II} in natural soil and sediment materials. Previous studies with a variety of synthetic and natural Fe^{III}–oxide-bearing solids have shown that Fe^{II} associated with mineralogically complex natural solids is much less efficient in catalyzing U^{VI} reduction than are pure-phase Fe^{III} oxides or natural materials rich in Fe^{III} oxide (Fredrickson et al., 2000; Finneran et al., 2002; Jeon et al., 2005). Jeon et al. (2005) suggested that heterogeneity in Fe^{II} binding sites, leading to lower average Fe^{II} sorption densities (e.g., in terms of the number of Fe^{II} atoms per square nanometer of solid surface) than in pure-phase oxide systems, was responsible for the observed inefficient abiotic reduction of U^{VI} in Fe^{II}-rich, mineralogically complex natural materials. The authors speculated that significantly lower Fe^{II} sorption density on natural materials could limit the ability of Fe^{II} and U^{VI} to achieve the surface coordination and subsequent orbital overlap required for efficient electron transfer. Lower Fe^{II} sorption densities are also consistent with lack of Fe^{II} oligomerization that, in view of the results of the present study, could explain the lower U^{VI}–Fe^{II} redox reactivity in natural materials. Alternatively, if conductivity through the oxide lattice between spatially separated U and Fe adsorbates controls the redox process, then direct Fe^{II}–Fe^{II} contact is not necessary for a two-electron transfer, and reactivity enhancement in pure-phase oxide systems comes by virtue of Fe and U atoms being adsorbed to the same crystallite. In the case of natural systems containing several phases, U^{VI} may be sorbed predominantly to one phase, whereas Fe^{II} may predominantly sorb to another, precluding lattice electron transfer between the redox centers. More detailed understanding of the relative importance of differences in electron conductivity vs. Fe^{II} surface coordination/speciation will be required to precisely define the controls on abiotic Fe^{II}-catalyzed U^{VI} reduction in soils and sediments.

5. CONCLUSIONS

Using a combination of pH titrations, uptake measurements, and XAFS spectroscopy, we were able to relate the Fe^{II}–U^{VI} redox reactivity in a carboxyl-surface environment to the molecular structure of the Fe and U species present in the system. Results show that aqueous and carboxyl-adsorbed Fe^{II} do not reduce carboxyl-adsorbed U^{VI} over at least 4 months. In contrast, complete, rapid reduction of U^{VI} to U^{IV} occurs under slightly higher pH conditions that favor Fe^{II} oligomerization. Because hydroxylation of the surface-adsorbed Fe^{II} species was excluded by the large-surface-area experiments as the reason for increased reactivity at higher pH, the latter was attributed to a facilitated two-electron transfer through the bonds of the Fe^{II} oligomer. Based on these results, we propose an Fe^{II}–U^{VI} redox mechanism that can explain the kinetic limitation of the homogeneous reaction, as well as the commonly observed high reactivity when an Fe^{III} oxide surface or structural Fe^{II} is present. The kinetic limitation in the case of monomeric Fe^{II} is attributed to formation of an unstable U^{V}–Fe^{III} intermediate complex that is not efficiently reduced by other Fe^{II} atoms in solution before it returns to the original Fe^{II} and U^{VI} species. The enhanced reactivity of oxide-adsorbed or structural Fe^{II} toward U^{VI} reduction is attributed to the ability of non-local Fe^{II} atoms to efficiently provide a second electron to an adsorbed U^{V} intermediate at the oxide surface through the bonds of the crystal. The ability of U^{VI} to obtain two electrons during a single complexation reaction may be an important, yet largely unconsidered, control on U^{VI} reduction.

Characterization of the Fe and U species in the system led to several unexpected results. U^{VI} appears to adsorb to the carboxyl surface at lower pH than the pH range where significant deprotonation of the surface occurs. At circumneutral pH, U^{VI} remains completely adsorbed to the carboxyl surface, whereas bulk stability constants predict predominance of hydrolysis oligomers in the system. These results suggest a significant electrostatic or steric component in the U-surface carboxyl binding energy and underscore the general need for careful characterization of the surface species. The observed inner-sphere adsorption of Fe^{II} to the carboxyl surface should cause increased reactivity of Fe^{II}, which was not observed with U^{VI} as the oxidant. Without the knowledge of Fe^{II} oligomerization at pH 8.4, the increased Fe^{II}–U^{VI} redox reactivity relative to pH 7.5 might normally be attributed to hydroxylation of the surface Fe^{II} species. However, the absence of U^{VI} reduction in the pH 8.4 high-surface-area system shows that hydroxylation of monomeric surface Fe^{II} species is not responsible for U^{VI} reduction in the pH 8.4 low-surface-area system.

Our study discerns some of the controls on U^{VI} reduction by Fe^{II} in a defined laboratory system. Although this system includes only a subset of all components present in natural environments, the factors considered in our study are expected to be significant in influencing the environmental fate of U. The presence of Fe^{II} in anoxic subsurface systems and its influence on contaminant transformations is well established. The carboxyl ligands, present as a surface in our system, are also present in nature in the form of humic acids, extracellular polymeric substances, and bacterial surfaces. Uranium in the environment will likely interact with Fe^{II} and carboxyl ligands in the subsurface, directly affecting U transport. The two-electron U^{VI} reduction mechanism inferred in our study is likely to be relevant to all forms of Fe^{II} present in environmental systems, such as Fe^{II} adsorbed to clays, Mn/Fe oxides, and bacteria, or structural Fe^{II} in clays, green rusts, and magnetite.

ACKNOWLEDGMENTS

We thank S. Traina at University of California-Merced for suggestions that greatly improved the manuscript. We also thank G. Zlateva for providing the TEM images; S. Kelly, B. Ravel, and the MRCAT staff for assistance in collecting the XAFS data; K. Haugen for editorial help. The constructive comments of three reviewers and the associate editor are also appreciated. Funding for this work was provided by the U.S. Department of Energy, Office of Science, Office of Biological and Environmental Research, Environmental Remediation Science Program (contract W-31-109-Eng-38), and the Environmental Molecular Science Institute at University of Notre Dame (funded by NSF Grant EAR-0221966). Work at the MR CAT beamline was supported by DOE under contract DE-FG02-94-ER45525 and the member institutions. Use of the APS was supported by the DOE Office of Science, Office of Basic Energy Sciences, under contract W-31-109-Eng-38.

APPENDIX A. SUPPLEMENTARY DATA

Detailed methods and materials section. Supplemental figures and tables. Supplementary data associated with this article can be found, in the online version, at doi:10.1016/j.gca.2007.01.025.

REFERENCES

Arden T. V. (1950) The solubility products of ferrous and ferrosic hydroxides. *J. Chem. Soc.*, 882–885.

Batson V. L., Bertsch P. M., and Herbert B. E. (1996) Transport of anthropogenic uranium from sediments to surface waters during episodic storm events. *J. Environ. Qual.* **25**(5), 1129–1137.

Becker U., Rosso K. M., and Hochella M. F. (2001) The proximity effect on semiconducting mineral surfaces: A new aspect of mineral surface reactivity and surface complexation theory? *Geochim. Cosmochim. Acta* **65**(16), 2641–2649.

Bell P. E., Mills A. L., and Herman J. S. (1987) Biogeochemical conditions favoring magnetite formation during anaerobic iron reduction. *Appl. Environ. Microbiol.* **53**(11), 2610–2616.

Beveridge T. J., and Murray R. G. E. (1980) Sites of metal deposition in the cell wall of *Bacillus subtilis*. *J. Bacteriol.* **141**(2), 876–887.

Blake R. L., Hessevick R. E., Zoltai T., and Finger L. W. (1966) Refinement of the hematite structure. *Am. Mineral.* **51**, 123–129.

Boyanov M. I. (2003) XAFS studies of metal-ligand interactions at organic surfaces and in solution. Ph.D. dissertation. Univ. of Notre Dame, IN.

Boyanov M. I., Kelly S. D., Kemner K. M., Bunker B. A., Fein J. B., and Fowle D. A. (2003) Adsorption of cadmium to *Bacillus subtilis* bacterial cell walls: a pH-dependent X-ray absorption fine structure spectroscopy study. *Geochim. Cosmochim. Acta* **67**(18), 3299–3311.

Buerge I. J., and Hug S. J. (1998) Influence of organic ligands on chromium(VI) reduction by iron(II). *Environ. Sci. Technol.* **32**(14), 2092–2099.

Buerge I. J., and Hug S. J. (1999) Influence of mineral surfaces on chromium(VI) reduction by iron(II). *Environ. Sci. Technol.* **33**(23), 4285–4291.

Chaudhuri S. K., Lack J. G., and Coates J. D. (2001) Biogenic magnetite formation through anaerobic biooxidation of Fe(II). *Appl. Environ. Microbiol.* **67**(6), 2844–2848.

Christensen A. N., Lehmann M. S., and Convert P. (1982) Deuteration of crystalline hydroxides - hydrogen-bonds of gamma-AlOO(H,D) and gamma-FeOO(H,D). *Acta Chem. Scand.* **36**(4), 303–308.

Cornell R. M., and Schwertman U. (1996) *The iron oxides: Properties, reactions, occurrences and uses*. Wiley, NewYork, pp. 340–343.

Docrat T. I., Mosselmans J. F. W., Charnock J. M., Whiteley M. W., Collison D., Livens F. R., Jones C., and Edmiston M. J. (1999) X-ray absorption spectroscopy of tricarbonatodioxouranate(V), [UO2(CO3)(3)](5-), in aqueous solution. *Inorg. Chem.* **38**(8), 1879–1882.

Doelsch E., Rose J., Masion A., Bottero J. Y., Nahon D., and Bertsch P. M. (2002) Hydrolysis of iron(II) chloride under anoxic conditions and influence of SiO4 ligands. *Langmuir* **18**(11), 4292–4299.

Ekstrom A. (1974) Kinetics and mechanisms of the disproportionation of uranium(V). *Inorg.Chem.* **13**(9), 2237–2241.

Elsner M., Schwarzenbach R. P., and Haderlein S. B. (2004) Reactivity of Fe(II)-bearing minerals toward reductive transformation of organic contaminants. *Environ. Sci. Technol.* **38**(3), 799–807.

Fein J. B., Daughney C. J., Yee N., and Davis T. A. (1997) A chemical equilibrium model for metal adsorption onto bacterial surfaces. *Geochim. Cosmochim. Acta* **61**(16), 3319–3328.

Finneran K. T., Anderson R. T., Nevin K. P., and Lovley D. R. (2002) Potential for bioremediation of uranium-contaminated aquifers with microbial U(VI) reduction. *Soil. Sediment. Contam.* **11**(3), 339–357.

Fischer A. (2003) Competitive coordination of the uranyl ion by perchlorate and water - the crystal structures of $UO_2(ClO_4)_2\cdot 3H_2O$ and $UO_2(ClO_4)_2\cdot 5H_2O$ and a redetermination of $UO_2(ClO_4)_2\cdot 7H_2O$. *Z. Anorg. Allg. Chem.* **629**(6), 1012–1016.

Forsyth J. B., Hedley I. G., and Johnson C. E. (1968) The magnetic structure and hyperfine field of goethite (alpha-FeOOH). *J. Phys. C: Solid State Phys.* **1**(1), 179–188.

Fredrickson J. K., Zachara J. M., Kennedy D. W., Dong H. L., Onstott T. C., Hinman N. W., and Li S. M. (1998) Biogenic iron mineralization accompanying the dissimilatory reduction of hydrous ferric oxide by a groundwater bacterium. *Geochim. Cosmochim. Acta* **62**(19–20), 3239–3257.

Fredrickson J. K., Zachara J. M., Kennedy D. W., Duff M. C., Gorby Y. A., Li S. M. W., and Krupka K. M. (2000) Reduction of U(VI) in goethite (alpha-FeOOH) suspensions by a dissimilatory metal-reducing bacterium. *Geochim. Cosmochim. Acta* **64**(18), 3085–3098.

Gorby Y. A., and Lovley D. R. (1992) Enzymatic uranium precipitation. *Environ. Sci. Technol.* **26**(1), 205–207.

Grenthe I., Fuger J., Konings R. J. M., Lemire R. J., Muller A. B., Nguyen-Trung C., Wanner, H. (1992) Chemical thermodynamics of uranium. North-Holland, Amsterdam.

Haim A. (1983) Mechanisms of electron-transfer reactions - the bridged activated complex. *Prog. Inorg. Chem.* **30**, 273–357.

Haskel D., Islam Z., Lang J., Kmety C., Srajer G., Pokhodnya K. J., Epstein A. J., and Miller J. S. (2004) Local structural order in the disordered vanadium tetracyanoethylene room-temperature molecule-based magnet. *Phys. Rev. B* **70**(5). Art. No. 054422.

Hudson E. A., Rehr J. J., and Bucher J. J. (1995) Multiple-scattering calculations of the uranium L(3)-edge X-ray absorption near-edge structure. *Phys. Rev. B* **52**(19), 13815–13826.

Ilton E. S., Haiduc A., Moses C. O., Heald S. M., Elbert D. C., and Veblen D. R. (2004) Heterogeneous reduction of uranyl by micas: crystal chemical and solution controls. *Geochim. Cosmochim. Acta* **68**(11), 2417–2435.

Ilton E. S., Haiduc A., Cahill C. L., and Felmy A. R. (2005) Mica surfaces stabilize pentavalent uranium. *Inorg. Chem.* **44**(9), 2986–2988.

Jeon B. H., Dempsey B. A., Royer R. A., and Burgos W. D. (2004) Low-temperature oxygen trap for maintaining strict anoxic conditions. *J. Environ. Eng.-ASCE* **130**(11), 1407–1410.

Jeon B. H., Dempsey B. A., Burgos W. D., Barnett M. O., and Roden E. E. (2005) Chemical reduction of U(VI) by Fe(II) at the solid-water interface using natural and synthetic Fe(III) oxides. *Environ. Sci. Technol.* **39**(15), 5642–5649.

Kelly S. D., Kemner K. M., Fein J. B., Fowle D. A., Boyanov M. I., Bunker B. A., and Yee N. (2002) X-ray absorption fine structure determination of pH-dependent U-bacterial cell wall interactions. *Geochim. Cosmochim. Acta* **66**(22), 3855–3871.

Kostka J. E., and Nealson K. H. (1995) Dissolution and reduction of magnetite by bacteria. *Environ. Sci. Technol.* **29**(10), 2535–2540.

Kubatko K. A. H., and Burns P. C. (2004) The crystal structure of a novel uranyl tricarbonate, $K_2Ca_3[(UO_2)(CO_3)_3]_2(H_2O)_6$. *Can. Mineral.* **42**, 997–1003.

Landa E. R., and Gray J. R. (1995) U.S. Geological Survey - research on the environmental fate of uranium mining and milling wastes. *Environ. Geol.* **26**(1), 19–31.

Langmuir D. (1978) Uranium solution-mineral equilibria at low temperatures with applications to sedimentary ore deposits. *Geochim. Cosmochim. Acta* **42**(6), 547–569.

Leussing D. L., and Kolthoff I. M. (1953) The solubility product of ferrous hydroxide and the ionization of the aquo-ferrous ion. *J. Am. Chem. Soc.* **75**(10), 2476–2479.

Liger E., Charlet L., and Van Cappellen P. (1999) Surface catalysis of uranium(VI) reduction by iron(II). *Geochim. Cosmochim. Acta* **63**(19–20), 2939–2955.

Lovley D. R., and Phillips E. J. P. (1992a) Bioremediation of uranium contamination with enzymatic uranium reduction. *Environ. Sci. Technol.* **26**(11), 2228–2234.

Lovley D. R., and Phillips E. J. P. (1992b) Reduction of uranium by *Desulfovibrio desulfuricans*. *Appl. Environ. Microbiol.* **58**(3), 850–856.

Lovley D. R., Stolz J. F., Nord G. L., and Phillips E. J. P. (1987) Anaerobic production of magnetite by a dissimilatory iron-reducing microorganism. *Nature* **330**(6145), 252–254.

Lutz H. D., Moller H., and Schmidt M. (1994) Lattice vibration spectra. 82. Brucite-type hydroxides M(OH)(2) (M = Ca, Mn, Co, Fe, Cd). IR and Raman spectra, neutron diffraction of Fe(OH)(2). *J. Mol. Struct.* **328**, 121–132.

Martell A. E., Smith R. M., Motekaitis R. J. (2001) NIST critically selected stability constants of metal complexes. U.S. Department of Commerce, National Institute of Standards and Technology.

Morosin B. (1978) Hydrogen uranyl phosphate tetrahydrate, a hydrogen-ion solid electrolyte. *Acta Crystallogr. Sect. B-Struct. Commun.* **34**(DEC), 3732–3734.

O'Loughlin E. J., Kelly S. D., Cook R. E., Csencsits R., and Kemner K. M. (2003) Reduction of uranium(VI) by mixed iron(II)/iron(III) hydroxide (green rust): formation of UO_2 nanoparticles. *Environ. Sci. Technol.* **37**(4), 721–727.

Renshaw J. C., Butchins L. J. C., Livens F. R., May I., Charnock J. M., and Lloyd J. R. (2005) Bioreduction of uranium: environmental implications of a pentavalent intermediate. *Environ. Sci. Technol.* **39**(15), 5657–5660.

Riley R. G., Zachara J. M., Wobber F. J. (1992) Chemical contaminants on DOE lands and selection of contaminant mixtures for subsurface science research. DOE/ER-0547T.U.S. Department of Energy.

Schwarzenbach R. P., Angst W., Holliger C., Hug S. J., and Klausen J. (1997) Reductive transformations of anthropogenic chemicals in natural and technical systems. *Chimia* **51**(12), 908–914.

Scott T. B., Allen G. C., Heard P. J., and Randell M. G. (2005) Reduction of U(VI) to U(IV) on the surface of magnetite. *Geochim. Cosmochim. Acta* **69**(24), 5639–5646.

Segre C. U., Leyarovska N. E., Chapman L. D., Lavender W. W., Plag P. W., King A. S., Kropf A. J., Bunker B. A., Kemner K. M., Dutta P., Duran R. S., and Kaduk J. (2000) The MRCAT insertion device beamline at the Advanced Photon Source. In *Synchrotron Radiation Instrumentation: Eleventh U.S. National Conference* Vol. CP521, (ed. P. Pianetta). American Institute of Physics, NewYork, pp. 419–422.

Sørensen J. (1982) Reduction of ferric iron in anaerobic, marine sediment and interaction with reduction of nitrate and sulfate. *Appl. Environ. Microbiol.* **43**(2), 319–324.

Sposito G. (2004) *The surface chemistry of natural particles*. Oxford University Press, New York.

Strathmann T. J., and Stone A. T. (2002) Reduction of oxamyl and related pesticides by Fe-II: influence of organic ligands and natural organic matter. *Environ. Sci. Technol.* **36**(23), 5172–5183.

Strathmann T. J., and Stone A. T. (2003) Mineral surface catalysis of reactions between Fe-II and oxime carbamate pesticides. *Geochim. Cosmochim. Acta* **67**(15), 2775–2791.

Stumm W. (1992) *Chemistry of the solid-water interface*. Wiley-Interscience, New York.

Stumm W., and Sulzberger B. (1992) The cycling of iron in natural environments - considerations based on laboratory studies of heterogeneous redox processes. *Geochim. Cosmochim. Acta* **56**(8), 3233–3257.

Templeton D. H., Zalkin A., Ruben H., and Templeton L. K. (1985) Redetermination and absolute configuration of sodium uranyl(VI) triacetate. *Acta Crystallogr. Sect. C-Cryst. Struct. Commun.* **41**(OCT), 1439–1441.

Wechsler B. A., Lindsley D. H., and Prewitt C. T. (1984) Crystal structure and cation distribution in titanomagnetites ($Fe_{3-x}Ti_xO_4$). *Am. Mineral.* **69**(7–8), 754–770.

Wehrli B., Sulzberger B., and Stumm W. (1989) Redox processes catalyzed by hydrous oxide surfaces. *Chem. Geol.* **78**(3–4), 167–179.

Wersin P., Hochella M. F., Persson P., Redden G., Leckie J. O., and Harris D. W. (1994) Interaction between aqueous uranium(VI) and sulfide minerals - spectroscopic evidence for sorption and reduction. *Geochim. Cosmochim. Acta* **58**(13), 2829–2843.

Williams A. G. B., and Scherer M. M. (2004) Spectroscopic evidence for Fe(II)–Fe(III) electron transfer at the iron oxide-water interface. *Environ. Sci. Technol.* **38**(18), 4782–4790.

Wyckoff R. W. G. (1960) *Crystal structures*. Interscience, New York.

Associate editor: Liane G. Benning